Supporting information

Oxygen affinity: the missing link enabling prediction of proton conductivities in doped barium zirconates

Yoshihiro Yamazaki,[1,2]* Akihide Kuwabara,[3] Junji Hyodo,[2] Yuji Okuyama,[4] Craig A.J. Fisher,[3] and Sossina M. Haile[5,6]

1 Kyushu University Platform of Inter/Transdisciplinary Energy Research (Q-PIT), Kyushu University, 744 Motooka, Fukuoka 819-0395, Japan
2 INAMORI Frontier Research Center, Kyushu University, 744 Motooka, Fukuoka 819-0395, Japan
3 Nanostructures Research Laboratory, Japan Fine Ceramics Center, 2-4-1 Mutsuno, Atsuta-ku, Nagoya, 456-8587, Japan
4 Department of Environmental Robotics, University of Miyazaki, 1-1 Gakuenkibanadai-nishi, Miyazaki 889-2192 Japan
5 Materials Science, California Institute of Technology, 1200 E. California Blvd., Pasadena, CA 91125, USA
6 Department of Materials Science and Engineering, Northwestern University, 2220 Campus Drive, Evanston, IL 60208, USA
* corresponding author: yamazaki@ifrc.kyushu-u.ac.jp

Computational Methodology
PAW potentials.

Table S1. Valence electron configurations and radial cut-offs of PAW potentials used in this study.

Element	Valence electrons	Radial cut-off (Å)
Ba	$5s^2\ 5p^6\ 6s^2$	2.80
Zr	$4s^2\ 4p^6\ 5s^2\ 4d^2$	2.50
O	$2s^2\ 2p^4$	1.52
Sc	$3s^2\ 3p^6\ 4s^2\ 3d^1$	2.50
Y	$4s^2\ 4p^6\ 5s^2\ 4d^1$	2.80
In	$4d^{10}\ 5s^2\ 5p^1$	2.50
Eu	$4f^7\ 5s^2\ 5p^6\ 6s^2$	2.80
Gd	$4f^7\ 5s^2\ 5p^6\ 5d^1\ 6s^2$	2.80
Er	$4f^{12}\ 5s^2\ 5p^6\ 6s^2$	2.60
Lu	$4f^{14}\ 5s^2\ 5p^6\ 5d^1\ 6s^2$	2.80

Dynamical stability of $BaZrO_3$. We performed first-principles lattice dynamics calculations using the Phonopy code[1] to investigate the dynamical stability of cubic $BaZrO_3$. Interatomic force constants were calculated in real space using 4 × 4 × 4 supercells of the $BaZrO_3$ unit cell, with the ***k***-point at (1/4 1/4 1/4) used for Brillouin zone sampling. Non-equivalent atomic displacements of 0.01 Å were employed for calculations of the force constants based on symmetry analyses. A non-analytical term correction was added to the dynamical matrices to include the longitudinal optical–transverse optical (LO-TO) splitting near the Γ point,[2,3] which requires knowledge of the Born effective charges of ions in $BaZrO_3$ and its dielectric constant. These were obtained using the linear response approach,[4] with the electronic and ionic parts of the dielectric constant calculated to be 4.87 and 59.67, respectively, giving a total of 64.54. Born effective charge tensors (Z^*) of Ba, Zr, and O ions were calculated to be

$$Z^*(\mathrm{Ba}) = \begin{pmatrix} 2.73 & 0 & 0 \\ 0 & 2.73 & 0 \\ 0 & 0 & 2.73 \end{pmatrix},$$

$$Z^*(\mathrm{Zr}) = \begin{pmatrix} 6.12 & 0 & 0 \\ 0 & 6.12 & 0 \\ 0 & 0 & 6.12 \end{pmatrix},$$

$$\text{and } Z^*(\mathrm{O}) = \begin{pmatrix} -4.86 & 0 & 0 \\ 0 & -1.99 & 0 \\ 0 & 0 & -1.99 \end{pmatrix}.$$

The Born effective charge tensor of O here corresponds to that of the atom located at (0 0.5 0.5) in the unit cell of cubic $BaZrO_3$.

The calculated phonon dispersion curve of cubic $BaZrO_3$ is shown in Fig. S1. All phonon branches have real frequencies (no soft modes). Our results are consistent with those of Bjørheim et al.[5] and A. Perrichon et al.[6], who also found that cubic $BaZrO_3$ is dynamically stable using PBE-type exchange-correlation potentials but with 2 × 2 × 2 supercells. These results confirm that the PBE potential successfully predicts the cubic form of $BaZrO_3$ to be the ground state under standard conditions.

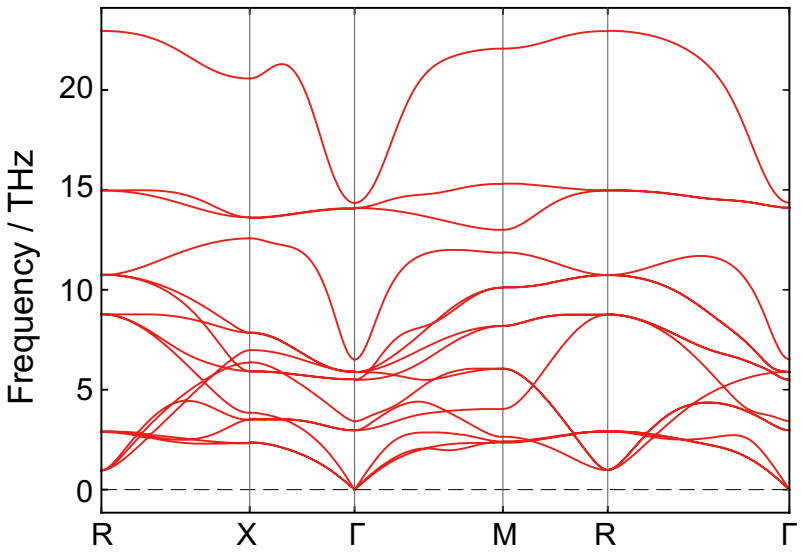

Figure S1. Phonon dispersion curves in the first Brillouin zone of cubic $BaZrO_3$ obtained from first-principles lattice dynamics calculations using a 4 × 4 × 4 supercell.

Correction for defect formation energies. The ideal total energy of the charged system, $E^*_{\mathrm{sup}}(D^q)$, was obtained from the sum of $E_{\mathrm{sup}}(D^q)$ and a correction term, $\Delta E_{\mathrm{sup}}(D^q)$, according to

$$E^*_{\mathrm{sup}}(D^q) = E_{\mathrm{sup}}(D^q) + \Delta E_{\mathrm{sup}}(D^q). \quad \text{(S1)}$$

Here, $\Delta E_{\mathrm{sup}}(D^q)$ can be expressed as[12-14]

$$\Delta E_{\mathrm{sup}}(D^q) = \frac{\alpha q^2}{2\epsilon L} - \frac{2\pi q Q}{3\epsilon L^3} + O(L^{-5}). \quad \text{(S1')}$$

The first term is the electrostatic Madelung energy of a point charge periodically embedded in a matrix of dielectric constant ε, and α and L are the Madelung constant of the supercell geometry and the average distance between defects under 3D periodic boundary conditions, respectively. For cubic systems like $BaZrO_3$, L is equal to the length of the supercell. We calculated the electronic and ionic parts of the dielectric constant of $BaZrO_3$ using density functional perturbation theory as described in the previous section. The value of ε, given by the sum of ionic and electronic contributions, was 64.54.

The second term in eq. S1' corresponds to a monopole-quadrupole interaction between a point charge and compensating background charges. Q is the second radial moment. However, it is difficult to directly determine Q in continuous crystalline systems after structural relaxation because regions between the embedded point charge and screening background charge cannot be separated completely. In the case of a trapped-proton system, in which an acceptor dopant (with effective negative charge) and a positively charged proton are together in the same system, although the net charge of the model is zero, the defect complex introduces a dipole moment, and dipole-dipole interactions occur between periodic images. Such dipole-dipole interactions show an L^{-3} dependence. The L^{-3} dependence term can be quantified by fitting to a series of defect formation energy calculations with different supercell sizes. The higher-order term, $O(L^{-5})$, was ignored in this study. In addition to the 625-atom (5 × 5 × 5) supercell models, 80-atom (2 × 2 × 2), 135-atom (3 × 3 × 3) and 320-atom (4 × 4 × 4) supercells were used to estimate the L^{-3} dependence terms. It should be noted that 80-atom supercells were not used for the trapped-proton systems, because 2 × 2 × 2 supercells are too small to be able to construct complexes with large distances between the dopant and proton. Sampling meshes of 3 × 3 × 3 and 2 × 2 × 2 ***k***-points using the Monkhorst-Pack scheme and one ***k***-point of (1/4 1/4 1/4) in the Brillouin zone were used for the 80-, 135- and 320-atom supercells, respectively.

E_{VBT} was obtained using $E_{\mathrm{VBT}} = E_{\mathrm{sup}}(\mathrm{perf}) - E_{\mathrm{sup}}(\mathrm{h}^{\bullet})$, where $E_{\mathrm{sup}}(\mathrm{h}^{\bullet})$ is the total energy of the perfect supercell with one hole in the topmost valence band. When the ***k***-points sampled in the supercell calculations differed from the ***k***-point of the VBT, a correction to E_{VBT}, ΔE_{VBT}, was added. The corrected VBT energy, E^*_{VBT}, was obtained from

$$E^*_{\mathrm{VBT}} = E_{\mathrm{VBT}} + \Delta E_{\mathrm{VBT}} = E_{\mathrm{VBT}} + (\varepsilon_{\boldsymbol{k}(\mathrm{VBT})} - \varepsilon_{\boldsymbol{k}(\mathrm{defect})}). \quad \text{(S2)}$$

where $\varepsilon_{\mathbf{k}(\mathrm{VBT})}$ is the highest occupied eigenenergy determined from the one-particle band structure in the Brillouin zone of the perfect supercell, and $\varepsilon_{\mathbf{k}(\mathrm{defect})}$ is the highest occupied

eigenenergy at the ***k***-points sampled in the defective supercell. For the positively-charged 80-atom perfect supercell, the hole was spread over several of the topmost valence bands. In this case, $\varepsilon_{\mathbf{k}(\text{defect})}$ was calculated according to

$$\varepsilon_{\boldsymbol{k}(\text{defect})} = \sum_i g_i \cdot \varepsilon_{\boldsymbol{k}(\text{band}),i}, \tag{S3}$$

where g_i is the hole occupancy of the ith band and $\sum_i g_i = 1$, and $\varepsilon_{\mathbf{k}(\text{band}),i}$ is the eigenenergy of the ith band of the defective supercell. Using this method, values of ΔE_{VBT} for the 80-, 135-, 320-, and 625-atom supercells were calculated to be 28, 69, 40, and 98 meV, respectively.

The chemical potential terms, μ_i, in eq. S1 were determined with reference to known phase equilibria. Based on the quasi-binary phase diagram of the BaO-ZrO_2 system by Gong et al.[7], we assumed two thermal equilibrium conditions. One was coexisting phases of $BaZrO_3$ and $Ba_3Zr_2O_7$ under BaO-rich (ZrO_2-poor) conditions, and the other was $BaZrO_3$ and ZrO_2 co-existing under ZrO_2-rich (BaO-poor) conditions. In addition to the solid phases, activities of the gaseous phases of H_2O and O_2 were also taken into account.

Under thermal equilibrium, chemical potentials of the constituent atoms in the coexisting phases are equal, so under BaO-rich conditions total energies (E) of $BaZrO_3$, $Ba_3Zr_2O_7$, H_2O and O_2 can be expressed as

$$\begin{cases} 3\mu_{\text{Ba}} + 2\mu_{\text{Zr}} + 7\mu_{\text{O}} = E(\text{Ba}_3\text{Zr}_2\text{O}_7) \\ \mu_{\text{Ba}} + \mu_{\text{Zr}} + 3\mu_{\text{O}} = E(\text{BaZrO}_3) \\ 2\mu_{\text{H}} + \mu_{\text{O}} = E\big(\text{H}_2\text{O(g)}\big) \\ 2\mu_{\text{O}} = E\big(\text{O}_2\text{(g)}\big) \end{cases}. \tag{S4}$$

Under ZrO_2-rich conditions, the first sub-equation in Eq. (S4) can be replaced by $\mu_{\text{Zr}} + 2\mu_{\text{O}} = E(ZrO_2)$. Under Zr-rich (Ba-poor) conditions, Ba deficiency is likely to occur. Ba deficiency is known to be detrimental to proton conductivity in $BaZrO_3$ systems.[15,16] We therefore only considered BaO-rich conditions in this work.

In order to fix the chemical potential of the dopant, an additional solid phase which contains the dopant element was calculated in addition to the compounds in eq. S4. The compounds calculated to determine the chemical potentials are summarized in Table S2. Calculating all total DFT energies of the phases on the RHS of eq. S4 allowed the necessary chemical potentials to be set. The present calculations correspond to systems at 0 K and 0 atm, so that the effects of finite temperature and pressure were not taken into account. Similar to the case of $BaZrO_3$, lattice constants of the coexisting solid phases were fully optimized using an initial cutoff energy of 500 eV. Total energies of each compound were then obtained by holding the lattice vectors fixed at their relaxed values performing calculations with a cutoff energy of 400 eV in which only the internal atomic positions were allowed to relax.

To model gaseous species O_2 and H_2O, a single molecule was placed in a vacuum-filled cell with fixed dimensions of $10 \times 10.5 \times 11$ Å^3, and the bond lengths of the molecules optimized using a cutoff energy of 400 eV and sampling only the Γ point of the first Brillouin zone.

Table S2. Calculated lattice constants of compounds other than $BaZrO_3$ used in this study compared with experiment.

Compound	$\boldsymbol{k}$-mesh	Lattice constants (Å) Calc.	Exp.	Ref.
$Ba_3Zr_2O_7$	6 × 6 × 2	a = 4.236 b = 4.236 c = 22.048	-	*
$Ba_3Sc_4O_9$	5 × 5 × 5	a = 5.847 c = 24.048	a = 5.7834 c = 23.6782	8
$Ba_3Y_4O_9$	3 × 3 × 3	a = 6.140 c = 25.598	a = 6.11 c = 25.187	9
$Ba_2In_2O_5$	4 × 4 × 4	a = 6.232 b = 16.883 c = 6.057	a = 6.0956 b = 16.7112 c = 5.9601	10
$BaEu_2O_4$	2 × 2 × 6	a = 10.601 b = 3.572 c = 12.454	a = 10.4968 b = 3.5362 c = 12.2902	11
$BaGd_2O_4$	2 × 2 × 6	a = 10.599 b = 3.532 c = 12.334	a = 10.4644 b = 3.5052 c = 12.2402	11
$Ba_3Er_4O_9$	3 × 3 × 3	a = 6.108 c = 25.385	a = 6.086 c = 25.077	12
$Ba_3Lu_4O_9$	3 × 3 × 3	a = 5.970 c = 24.687	a = 6.03 c = 24.753	13

* To the best of our knowledge, experimental lattice constants of $Ba_3Zr_2O_7$ have not been reported. A hypothetical model for $Ba_3Zr_2O_7$ was constructed by replacing Sr with Ba in the unit cell of $Sr_3Zr_2O_7$ reported in ref. 14 and fully relaxing the structure.

Figure S2 shows plots of the calculated defect formation energies of individual point defects and protons on the 1st NP site against inverse supercell volume, L^{-3}, under BaO-rich conditions when E_{VBT} = 0. Madelung energy corrections are included in the values plotted for single-defect models. $E^*(D^q)$ as obtained by linear extrapolation to zero on the horizontal axis. In these plots, the deviation from linear dependence on L^{-3} of the formation energies appears greater for the single defects than the associated defects. One possible reason for this may be differences in the accuracy of the calculated energies as a result of using different $\boldsymbol{k}$-mesh densities for supercells of different sizes.

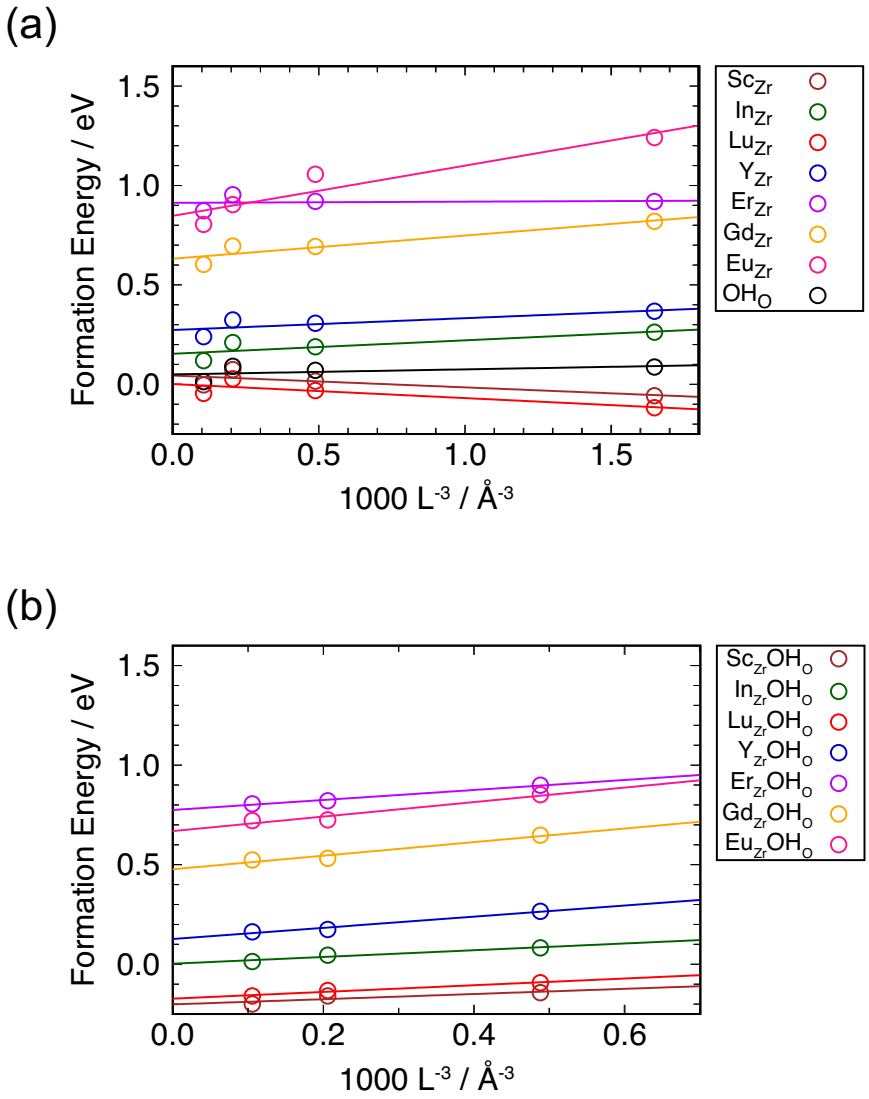

Figure S2. Defect formation energies of (a) single defects, and (b) protons trapped on 1st nearest proton sites in $BaZrO_3$ vs inverse supercell volume, L^{-3}.

Hydration and proton-dopant association energies. Acceptor doping of $BaZrO_3$ at elevated temperatures produces a solid solution with oxide-ion vacancies forming to maintain charge balance. In humid atmospheres at low temperature, protons can be incorporated into the $BaZrO_3$ lattice via hydration reactions involving these vacancies. Protons tend to become associated with acceptor dopants because their opposite effective charge states leads to coulombic attraction. In the case of Y-doped $BaZrO_3$, these defect reactions can be expressed using Kröger-Vink notation as

$$\mathrm{Y_{Zr}^{\prime}} + \{\mathrm{Y_{Zr}}V_{\mathrm{O}}\}^{\bullet} + \mathrm{H_2O}(g) \rightarrow 2\{\mathrm{Y_{Zr}OH_O}\}^{\times}. \quad \text{(S5)}$$

$$\mathrm{Y_{Zr}^{\prime}} + \mathrm{OH_O^{\bullet}} \rightarrow \{\mathrm{Y_{Zr}OH_O}\}^{\times}. \quad \text{(S6)}$$

Here we focus on the hydration occurring in the vicinity of acceptor dopants. The hydration energy, E_{hyd}, and the proton-dopant association energy, E_{as}, were calculated respectively according to the equations

$$E_{\mathrm{hyd}} = 2E_{\mathrm{f}}(\{\mathrm{Y_{Zr}OH_O}\}^{\times}) - \left(E_{\mathrm{f}}\left(\mathrm{Y_{Zr}^{\prime}}\right) + E_{\mathrm{f}}(\{\mathrm{Y_{Zr}}V_{\mathrm{O}}\}^{\bullet})\right) \quad \text{(S7)}$$

and

$$E_{\mathrm{as}} = E_{\mathrm{f}}(\{\mathrm{Y_{Zr}OH_O}\}^{\times}) - \{E_{\mathrm{f}}\left(\mathrm{Y_{Zr}^{\prime}}\right) + E_{\mathrm{f}}(\mathrm{OH_O^{\bullet}})\}. \quad \text{(S8)}$$

Using eq. 1 in the main text, each of the defect formation energies on the RHS of eq. S7 and S8 can be expanded as

$$E_{\mathrm{f}}(\{\mathrm{Y_{Zr}OH_O}\}^{\times}) = E^{*}_{\mathrm{sup}}(\{\mathrm{Y_{Zr}OH_O}\}^{\times}) - E_{\mathrm{sup}}(\mathrm{perf}) - \mu_{\mathrm{Y}} + \mu_{\mathrm{Zr}} - \mu_{\mathrm{H}}, \quad \text{(S9)}$$

$$E_{\mathrm{f}}\left(\mathrm{Y_{Zr}^{\prime}}\right) = E^{*}_{\mathrm{sup}}\left(\mathrm{Y_{Zr}^{\prime}}\right) - E_{\mathrm{sup}}(\mathrm{perf}) - \mu_{\mathrm{Y}} + \mu_{\mathrm{Zr}} - (E_{\mathrm{fermi}} + E^{*}_{\mathrm{VBT}}), \quad \text{(S10)}$$

$$E_{\mathrm{f}}(\{\mathrm{Y_{Zr}}V_{\mathrm{O}}\}^{\bullet}) = E^{*}_{\mathrm{sup}}(\{\mathrm{Y_{Zr}}V_{\mathrm{O}}\}^{\bullet}) - E_{\mathrm{sup}}(\mathrm{perf}) - \mu_{\mathrm{Y}} + \mu_{\mathrm{Zr}} + \mu_{\mathrm{O}} + (E_{\mathrm{fermi}} + E^{*}_{\mathrm{VBT}}), \quad \text{(S11)}$$

and

$$E_{\mathrm{f}}(\mathrm{OH_O^{\bullet}}) = E^{*}_{\mathrm{sup}}(\mathrm{OH_O^{\bullet}}) - E_{\mathrm{sup}}(\mathrm{perf}) - \mu_{\mathrm{H}} + (E_{\mathrm{fermi}} + E^{*}_{\mathrm{VBT}}). \quad \text{(S12)}$$

Inserting these into eqns. S7 and S8 gives

$$E_{\mathrm{hyd}} = 2E^{*}_{\mathrm{sup}}(\{\mathrm{Y_{Zr}OH_O}\}^{\times}) - \left(E^{*}_{\mathrm{sup}}\left(\mathrm{Y_{Zr}^{\prime}}\right) + E^{*}_{\mathrm{sup}}(\{\mathrm{Y_{Zr}}V_{\mathrm{O}}\}^{\bullet}) + \mu_{\mathrm{H_2O}}\right) \quad \text{(S13)}$$

and

$$E_{\mathrm{as}} = E^{*}_{\mathrm{sup}}\left(\mathrm{Y_{Zr}^{\prime}}\right) + E^{*}_{\mathrm{sup}}(\mathrm{OH_O^{\bullet}}) - \left[E^{*}_{\mathrm{sup}}(\{\mathrm{Y_{Zr}OH_O}\}^{\times}) + E_{\mathrm{sup}}(\mathrm{perf})\right]. \quad \text{(S14)}$$

This shows that terms related to the Fermi energy are cancelled out in the calculation of E_{hyd} and E_{as}. (A correction is only needed for systems with a net charge.)

We measured the association energy of Y-doped $BaZrO_3$ experimentally to be -0.30 eV,[17] which means that the present calculation underestimates the association energy slightly. There are several possible reasons for this difference. For example, in the experimental measurements, the acceptor dopant concentration was 20 at%, whereas in our DFT calculations the dopants are at the dilute limit, so the calculated association energies correspond to a simple 2-body interaction between dopant and proton. More complex defect clusters that occur at higher dopant concentrations likely affect the strength of proton trapping to some degree and thus association energies in the $BaZrO_3$ system. Another important difference is that our calculations correspond to materials at 0 K, so that thermal effects such as ion vibration and thermal lattice expansion are not included. More accurate calculations will require use of more computationally expensive methods to be used such as *ab initio* molecular dynamics, which is beyond the scope of this work.

We also calculated the Coulomb potential energy between a trivalent dopant (effective charge -1) and proton (effective charge +1) on the 11th nearest proton site using the calculated relative dielectric constant for $BaZrO_3$, 64.54. The potential energy, $E_{C.11th}$, in this case was -0.027 eV, which represents the Coulombic contribution to the association energy of all the dopants examined. This value is smaller than the association energies for protons on this site for all dopant species, with a greater decrease in energy with larger dopant size; e.g., $E_{as.11th}$ for Sc and Eu were calculated to be -0.062 eV and -0.133 eV, respectively. These results show that lattice distortion (strain) caused by the dopant extends at least to a distance of around 9 Å from the dopant, and can be four or five times greater than the Coulomb potential for larger dopants.

Dopant-oxygen affinities, hydrogen affinities, and hypothetical hydration energies in $BaZrO_3$

As mentioned in the main text, we break down the hydration reaction in the vicinity of an acceptor dopant into three elementary reactions, viz., occupation of oxygen vacancy sites, direct proton incorporation, and association between proton and dopant (eqns. S15, S16, and S17, respectively):

$$\{Y_{Zr}V_O\}^{\bullet} + 1/2O_2(g) \rightarrow Y_{Zr}^{\prime} + O_O^{\times} + 2h^{\bullet} \quad \text{(S15)}$$

$$O_O^{\times} + \frac{1}{2}H_2(g) + h^{\bullet} \rightarrow OH_O^{\bullet} \quad \text{(S16)}$$

$$Y_{Zr}^{\prime} + OH_O^{\bullet} \rightarrow \{Y_{Zr}OH_O\}^{\times} \quad \text{(S17)}$$

Energies of eqns. S15 and S16, respectively, can be described as dopant-oxygen and hydrogen-oxygen affinities, or oxygen and hydrogen affinities for short, and the energy of eq. S17 is the dopant-proton association energy. The oxygen affinity, $E_{O.dopant}$, and $E_{H.host}$, are written in terms of DFT energies in eqns. S18 and S19, respectively:

$$E_{O.dopant} = E_f\left(Y_{Zr}^{\prime}\right) - E_f(\{Y_{Zr}V_O\}^{\bullet}) \quad \text{(S18)}$$

$$E_{H.host} = E_f(OH_O^{\bullet}) \quad \text{(S19)}$$

Using eq. 1 of the main text, the defect formation energies on the RHS of eqns. S18 and 19 can be expanded as

$$E_{\mathrm{O.dopant}} = E^{*}_{\mathrm{sup}}\left(\mathrm{Y}^{\prime}_{\mathrm{Zr}}\right) + 2E_{\mathrm{sup}}(\mathrm{h}^{\bullet}) - \{E^{*}_{\mathrm{sup}}((\mathrm{Y}_{\mathrm{Zr}}V_{\mathrm{O}})^{\bullet}) + 2E_{\mathrm{sup}}(\mathrm{per}) + 2(\Delta E_{\mathrm{VBT}} + E_{\mathrm{fermi}}) + \mu_{\mathrm{O}}\} \quad \text{(S20)}$$

$$E_{\mathrm{H.host}} = E^{*}_{\mathrm{sup}}(\mathrm{OH}^{\bullet}_{\mathrm{O}}) + (\Delta E_{\mathrm{VBT}} + E_{\mathrm{fermi}}) - \left\{E_{\mathrm{sup}}(\mathrm{h}^{\bullet}) + \mu_{\mathrm{H}}\right\} \quad \text{(S21)}$$

$$E_{\mathrm{hyd.free}} = E^{*}_{\mathrm{sup}}\left(\mathrm{Y}^{\prime}_{\mathrm{Zr}}\right) + 2E^{*}_{\mathrm{sup}}(\mathrm{OH}^{\bullet}_{\mathrm{O}}) - \{E^{*}_{\mathrm{sup}}((\mathrm{Y}_{\mathrm{Zr}}V_{\mathrm{O}})^{\bullet}) + 2E_{\mathrm{sup}}(\mathrm{perf}) + \mu_{\mathrm{H_2O}})\} \quad \text{(S22)}$$

As seen from eqns. S15 and S16, oxygen and hydrogen affinities depend on the energy of formation of holes, and thus their energies depend on the Fermi energy level within the band gap. In this study, we assumed that the Fermi level was located at the valence band top, which corresponds to the *p*-type limit at 0 K.

Nearest-proton sites to a dopant atom

The 16 different proton sites relative to a dopant atom in a 5×5×5 supercell of $BaZrO_3$ identified from first-principles calculations are illustrated in Fig. S3.

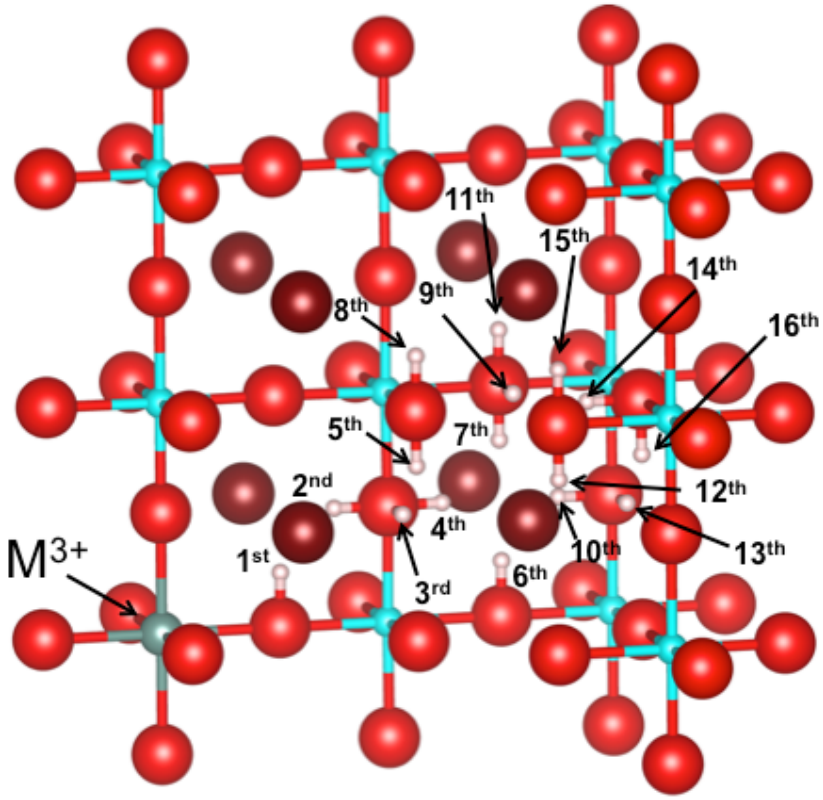

Figure S3. The 16 different proton sites in a 5×5×5 supercell of cubic $BaZrO_3$, relative to an M^{3+} acceptor dopant atom, used for *ab initio* calculations of proton-dopant association energies.

Results

Proton conductivities versus dopant ion radius

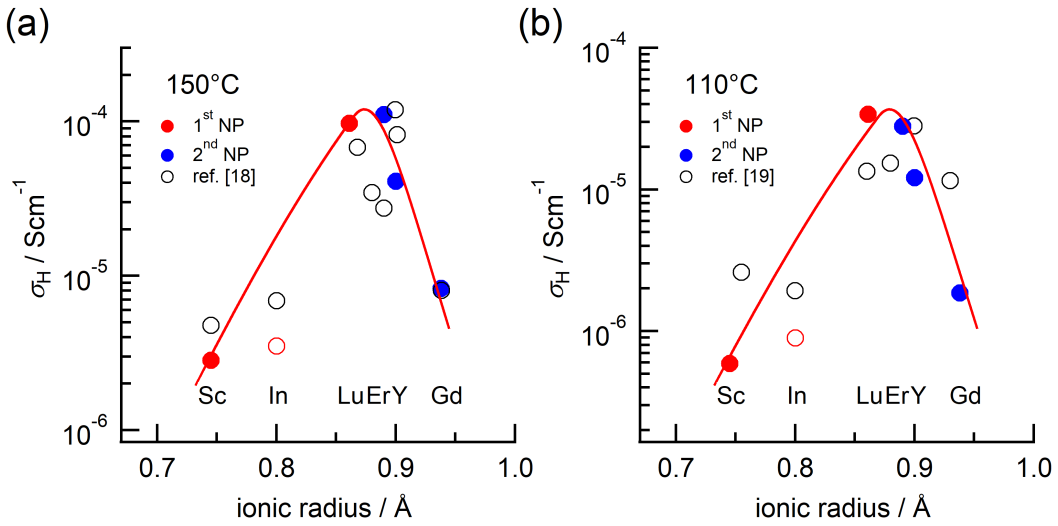

Figure S4. Proton conductivities, σ_H, at (a) 150 °C and (b) 110 °C in 20 at% doped barium zirconates compared with results from refs. 18 and 19 determined in 15 and 20 at% dopant concentration, respectively.

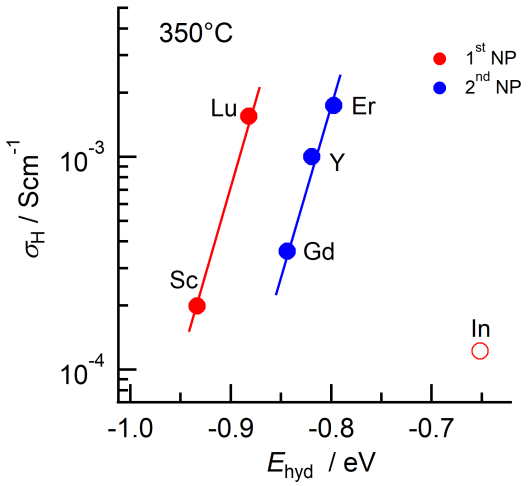

Figure S5. Proton conductivities, σ_H, at 350 °C against calculated hydration energy, E_{hyd}. The conductivities were determined in the 20 at% doped barium zirconates.

References

1 Togo, A. & Tanaka, I. First principles phonon calculations in materials science *Scr. Mater.*, 108, 1–5 (2015)

2 Gonze, X., Charlier, J.-C., Allan, D.C., & Teter, M. P. Interatomic force constants from first principles: The case of α-quartz. *Phys. Rev. B* 50, 13035(R) (1994)

3 Gonze, X., & Lee, C. Dynamical matrices, Born effective charges, dielectric permittivity tensors, and interatomic force constants from density-functional perturbation theory. *Phys. Rev. B* 55, 10355 (1997)

4 Gajdoš, M., Hummer, K., Kresse, G., Furthmüller, J. & Bechstedt, F. Linear optical properties in the projector-augmented wave methodology. *Phys. Rev. B* 73, 1–9 (2006).

5 Bjørheim, T. S., Kotomin, E. A. & Maier, J. Hydration entropy of $BaZrO_3$ from first principles phonon calculations. *J. Mater. Chem. A* 3, 7639–7648, 2015.

6 Perrichon, A., Granhed, E. J., Romanelli, G., Piovano, A., Lindman, A., Hyldgaard, P., Wahnström, G., & Karlsson M. Unraveling the Ground-State Structure of $BaZrO_3$ by Neutron Scattering Experiments and First-Principles Calculations. *Chem. Mater.* 32, 2824–2835, 2020

7 Gong, W. P., Chen, T. F. & Jin, Z. P. Thermodynamic investigation of ZrO_2-BaO system. *Trans. Nonferrous Met. Soc. China* (English Ed. 17, 232–237 (2007).

8 Spitsyn, V. I., Kovba, L. M., Paromova, M. V., Yudinskaya, I. V. & Prokofeva, I. G. Double oxide of barium and rare-earth elements. *Dokl. Akad. Nauk SSSR* 180, 879–881 (1968).

9 Szymanik, B. Structure and decomposition of ceramic $Ba_3Y_4O_9$. *Solid State Ionics* 109, 223–228 (1998).

10 Gregory, D. H. & Weller, M. T. Phases in the System $Ba_2M_{2-x}Cu_xO_{4+\delta}$, M = In, Sc: Structure and Oxygen Stoichiometry. *J. Solid State Chem.* 107, 134–148 (1993).

11 Besara, T. et al. Single crystal synthesis and magnetism of the $BaLn_2O_4$ family (Ln = lanthanide). *Prog. Solid State Chem.* 42, 23–36 (2014).

12 Müller-Buschbaum, H. & Schrandt, O. Zur kristallstruktur von $Ba_3Ln_4O_9$ (Ln = Dy, Er, Y,Yb). *J. Alloys Compd.* 191, 151–154 (1993).

13 Krüger, J. & Müller-Buschbaum, H. $Ba_3Lu_4O_9$: Synthese und Strukturuntersuchung. *Z. Anorg. Allg. Chem.* 512, 59–64 (1984).

14 Longo, V. & Minichelli, D. La struttura cristallina di $Sr_3Zr_2O_7$, ortorombico. *Ceramurgia* 4, 25–28 (1974).

15 Yamazaki, Y., Hernandez-Sanchez, R. & Haile, S. M. Cation non-stoichiometry in yttrium-doped barium zirconate: phase behavior, microstructure, and proton conductivity. *J. Mater. Chem.* 20, 8158–8166 (2010)

16 Han, D., Kishida, K., Inui H., & Uda T. Substantial appearance of origin of conductivity decrease in Y-doped $BaZrO_3$ due to Ba-deficiency. *RSC Adv.*, 4 31589–31593 (2014).

17 Yamazaki, Y., Blanc, F., Okuyama, Y., Buannic, L., Lucio-Vega, J. C., Grey, C. P., Haile, S. M., Proton trapping in yttrium-doped barium zirconate. *Nat. Mater.* 12, 647-651 (2013).

18 Imashuku, S., Uda, T., Nose, Y., Taniguchi, G., Ito, Y., Awakura, Y., Dependence of Dopant Cations on Microstructure and Proton Conductivity of Barium Zirconate. *J. Electrochem. Soc.* 156, B1–B8 (2009).

19 Gilardi, E., Fabbri, E., Bi, L., Rupp, J. L. M., Lippert, T., Pergolesi, D., Traversa, E., Effect of Dopant-Host Ionic Radii Mismatch on Acceptor -Doped Barium Zirconate Microstructure and Proton Conductivity. *J. Phys. Chem. C* 121, 9739–9747 (2017).